In Vitro Polyphenolics Erythrocyte Model and in Vivo Chicken Embryo Model Revealed Gallic Acid to Be a Potential Hemorrhage Inducer: Physicochemical Action Mechanisms

ARTICLE *in* CHEMICAL RESEARCH IN TOXICOLOGY · FEBRUARY 2013

Impact Factor: 3.53 · DOI: 10.1021/tx300456t · Source: PubMed

Chemical Research in Toxicology

Article

pubs.acs.org/crt

In Vitro Polyphenolics Erythrocyte Model and *in Vivo* Chicken Embryo Model Revealed Gallic Acid to Be a Potential Hemorrhage Inducer: Physicochemical Action Mechanisms

Yaw-Bee Ker,[†,○] Chiung-Chi Peng,[‡,○] Chien-Hong Lin,[§] Kuan-Chou Chen,*[,∥,⊥] Chiu-Lan Hsieh,*[,§] and Robert Y. Peng*[,#]

[†]Department of Applied Food Technology, Hungkuang University, 34 Chung-Chie Road, Shalu County, Taichung Hsien, Taiwan 433

[‡]Graduate Institute of Clinical Medicine, College of Medicine, Taipei Medical University, 250 Wu-shing Street, Taipei, Taiwan 11031

[§]Graduate Institute of Biotechnology, Changhua University of Education, 1 Jin-De Road, Changhua, Taiwan 50007

[∥]Department of Urology, School of Medicine, College of Medicine, Taipei Medical University, 250, Wu-shing Street, Taipei, Taiwan 11031

[⊥]Department of Urology, Shuang Ho Hospital, Taipei Medical University, 291, Zhongzheng Road, Zhonghe, Taipei, Taiwan 23561

[#]Research Institute of Biotechnology, Hungkuang University, 34 Chung-Chie Road, Shalu County, Taichung Hsien, Taiwan 433

ABSTRACT: The *in vivo* chicken embryo model (CEM) demonstrated that gallic acid (GA) induced dysvascularization and hypoxia. Inflammatory edema, Zenker's necrosis, hemolysis, and liposis of cervical muscles were the common symptoms. Levels of the gene *hif-1α*, HIF-1α, TNF-α, IL-6, and NFκB in cervical muscles were all significantly upregulated, while the vascular endothelial growth factor (VEGF) was downregulated in a dose-responsive manner. Consequently, the cervical muscle inflammation and hemolysis could have been stimulated en route to the tissue TNF-α-canonical and the atypical pathways. We hypothesized that GA could deplete the dissolved oxygen (DO) at the expense of semiquinone and quinone formation, favoring the reactive oxygen species (ROS) production to induce RBC disruption and Fe^{2+} ion release. To explore this, the *in vitro* polyphenolics-erythrocyte model (PEM) was established. PEM revealed that the DO was rapidly depleted, leading to the release of a huge amount of Fe (II) ions and hydrogen peroxide (HPO) in a two-phase kinetic pattern. The kinetic coefficients for Fe (II) ion release ranged from 0.347 h^{-1} to 0.774 h^{-1}; and those for Fe (III) ion production were from 6.66×10^{-3} h^{-1} to 8.93×10^{-3} h^{-1}. For phase I HPO production, they ranged from 0.236 h^{-1} to 0.774 h^{-1} and for phase II HPO production from 0.764 h^{-1} to 2.560 h^{-1} at GA within 6 μM to 14 μM. Thus, evidence obtained from PEM could strongly support the phenomena of CEM. To conclude, GA tends to elicit hypoxia-related inflammation and hemolysis in chicken cervical muscles through its extremely high prooxidant activity.

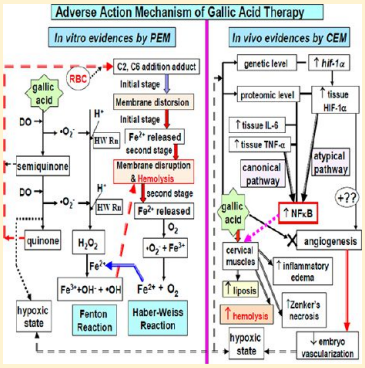

■ INTRODUCTION

Gallic acid (3,4,5-trihydroxybenzoic acid) (GA) is widely distributed in various plants, fruits, and foods and extensively used as a therapeutic adjuvant in antibacterials, antivirals, and anticancers.[1,2] Qiu et al. reported that GA was toxic against cultured vascular smooth muscle cells (VSMCs).[3] GA treatment elicited growth inhibition and death of human umbilical vein endothelial cells (HUVECs).[2] GA was reported to be one of the active angiogenesis inhibitors present in *Rubus* leaf extract. At a dose of 0.1% w/w i.p., GA caused a 41% inhibition of angiogenesis.[4] Previously, GA was shown to be potentially teratogenic and able to suppress angiogenesis in the chicken embryo model (CEM).[5] The main symptoms mostly encountered were inflammation, edema, hemorrhage, and liposis of the *musculus longissimus cervicis* (the cervical muscle) and erythrocyte hemolysis.[5]

GA decreased or increased reactive oxygen species levels, depending on the dose and the cell type tested. GA exhibits both prooxidant and antioxidative properties depending on the presence of iron or hydrogen peroxide in the medium and plasma.[6,7] Superoxide anions, H_2O_2, and gallyl quinones are rapidly produced nonenzymatically by autoxidation of GA in physiological solutions.[8] Moderate H_2O_2 levels decreased vascular tone, but high H_2O_2 and quinone levels caused irreversible relaxations due to cellular damage.[8] In addition, gallic acid inhibited the growth and proliferation of testicular cells and increased the intracellular level of hydrogen peroxide in mouse spermatogonia.[9]

We hypothesized that some organs that are actively responsible for oxygen transport such as the erythrocytes

Received: November 14, 2012
Published: February 14, 2013

could be the most delicate target of GA, which may lead to depletion of dissolved oxygen and severe hypoxia. Alternatively, the quinones can destroy the membranes and alter the permeability of cells through the formation of the peptide−quinone adducts. The released ferrous ion from the erythrocytes may elicit coupling of the Haber−Weiss reaction and Fenton reaction to produce huge amounts of hydrogen peroxide, which may further disintegrate the erythrocytes. Thus, we developed the *in vitro* polyphenolics erythrocyte model to confirm our hypothesis.

EXPERIMENTAL PROCEDURES

Chemicals. Gallic acid was obtained from Dainippon Pharmaceutical Co., Ltd. (Osaka, Japan) as a yellowish−white crystalline powder with a purity of over 98%. Normal saline was purchased from China Pharmaceutical and Chemical Co. (Taipei, Taiwan).

Rabbit antibodies to cervical muscle tissue vascular endothelial growth factor (VEGF) (1:1000), tumor necrotic factor (TNF)-α (1:1000), hypoxia inducible factor (HIF)-1α, and β-actin (1:500), the secondary antibodies, the cell lysis buffer, and the protein lysis buffer were provided by Santa Cruz Biotechnology (Santa Cruz, CA, USA). ELISA interleukin-6 (IL-6) and hydrogen peroxide kits were supplied by R&D System (Minneapolis, MN, USA). The Safe View DNA stain was purchased from Applied Biological Materials Inc. (BC, Canada). All other reagents were from Invitrogen (Invitrogen Life Technologies, CA, USA) unless otherwise stated.

***In Vivo* Chicken Embryo Model (CEM).** *Stage Determination and Application of Gallic Acid.* According to the Hamilton−Hamburger stage guidance (1992),[10] the somite formation and neural folds occur early from stage 7 to stage 21, which corresponds to 23 h to day 3.5. Blood islands with 4 somites develop at stage 8 (26−29 h); consequently, we set the observation point on day 5.5 for examination of the status of vascularization in embryos, while day-1 chicks were selected for the investigation of the pathological changes and tissue proinflammatory cytokines.

Briefly, 60 day-1 fertilized Leghorn eggs, each weighing 47.5−55.6 g, were purchased from Qing-Dang Chicken Farm (Taichung, Taiwan). These eggs were divided into 5 major groups, with 12 eggs in each: Group 1, PBS control; Group 2, 2 μM GA; Group 3, 6 μM GA; Group 4, 10 μM GA; and Group 5, 14 μM GA. These fertilized eggs purchased from the farmer were immediately placed in an incubator (Haw-Yang Agricultural Farm, Taichung, Taiwan) and incubated at 37 °C, RH 70−80% for 1.5 days (HH stage 10). To apply GA, these eggs were moved to a laminar flow chamber. On the egg shell, a hole of size 2 × 2 mm^2 was aseptically drilled through with a pin-driller. The embryos were then moved as close as to the hole openings by carefully turning them around before the observer's eyes and a direct strong light source. PBS and the required amount of GA were applied using a pippetman to obtain a final concentration of 0, 2, 6, 10, and 14 μM of GA, respectively, in each group. After administration, the openings were immediately sealed aseptically with a 3 M tape. The incubation was continued at 37 °C and RH 70−80%. The check points were set on day-5.5 (embryos) and day-1 (chicks).[10] All tools and apparatuses were previously aseptically sterilized before all operations.

Sample Tissue Collection. The day 5.5 (stage 28) embryos and the cervical muscles of day-1 chicks were collected and immediately rinsed with normal saline (0.92%, pH 7.4) three times. The specimens were placed in microcentrifuge tubes and stored at −80 °C or directly immersed in 12% neutral buffered formalin for pathological examination.

Image Determination of Vascularization. The day 5.5 (stage 28) embryos were obtained by carefully removing the shells. Briefly, the embryos were placed on the Petri dishes with the embryos positioned at the center point of the egg yolk surface and photographed. The extent of vascularization around the embryos was analyzed by the software Image-Pro Plus 6.0. The vascular distribution in the specific area centered with the embryo was determined and the degree of vascularization was expressed in percent area of vascularization in the total area of the image exposed for analysis.[11]

Histopathological Examination. The tissue specimens were fixed in 10% neutral buffered formalin at 1: 25 ratio for 48 h. The histopathological examination with Hematoxylin and Eosin stain was conducted according to the conventional HE stain protocol by Courtesy of Dr. C. W. Liaw, Associate Professor of The Animal Disease Diagnosis Center, Chung-Hsing University, Taichung, Taiwan.

Protein Extraction from the Tissues. Lysis buffer (10 mL) was mixed with 100 μL of protease inhibitor and mixed well (protein inhibitor lysis buffer, PILB). To 200 mg of cervical muscle of chicks or embryo tissues frozen on the ice chips, 1 mL of PILB was added. The mixture was homogenized and centrifuged at 4 °C 14000*g* for 20 min. The supernatant was separated and transferred to a new microcentrifuge tube. The mixture containing the whole intracellular proteins was stored at −80 °C for use. The pellet residue was used for extraction of the nuclear proteins.

Protein Extraction from the Nuclei. To the pellets, 400 μL of 10 mM Tris-HCl (pH 7.5, containing 10 mM NaCl) was added. The mixture, stirred to disperse the pellets, was centrifuged at 4 °C and 1300*g* for 10 min. The supernatant was removed and discarded. To the sediment, 150 μL of extraction buffer (50 mM HEPES, pH 7.5, containing 420 mM NaCl, 0.5 mM EDTA, 0.1 mM EGTA, and 10% glycerol) was added to suspend the pellets. The mixture was sonicated for 1 min and centrifuged at 4 °C and 10000*g* for 10 min. The supernatant was separated and stored at −80 °C for use.

Western Blot. *Preparation of SDS−PAGE.* The required preparation of the gel for SDS−PAGE is according to the protein size in the problem. Therefore, 7.5% of the gel for SDS−PAGE as the bottom layer was poured into the glass chamber of the electrophoretic apparatus. Ethanol (75%) was used to make the surface even while pressing. After SDS−PAGE, the gel became coagulated, and the ethanol was decanted. Separately, 4% of the gel for SDS−PAGE was topped onto the previous bottom layer. The electrophoretic joint chamber was set in and the gel allowed to coagulate. The sample and the reference proteins to be determined were applied into the chamber. A potential 75 V was applied, and the electrophoresis was started for 3 h.

Protein Transfer. After the electrophoresis was completed, the SDS−PAGE gel was immersed into the transfer buffer (50 mM Tris, 40 mM glycine, 0.375% SDS, pH 9.0−9.4, and 20% methanol). Alternatively, the PVDF membrane was immersed in methanol for 5 min and then together with filter paper immersed in transfer buffer. The transfer order was sponge, filter paper, SDS−PAGE, PVDF membrane, filter paper, and then sponge. The formation of gas bubbles between the SDS−PAGE and PVDF membrane was carefully avoided and eliminated. Protein transfer was conducted in the wet transfer chamber (Bio-Rad) at 100 V for 60 min to carry out the transfer of protein onto the PVDF membrane. The PVDF membrane was peeled off and dipped into 5% skimmed milk at 4 °C in a refrigerator for 24 h.

Chemiluminescence Enhanced Antibody Hybridization and Images. All of the protocol was conducted by following the manufacturer's instructions. Briefly, the PVDF membrane was immersed in primary antibodies (HIF-1α, TNF-α, VEGF, NFκB, and β-actin, all 1:1000) for 2 h at ambient temperature and then rinsed three times with PBST buffer (containing 0.05% Tween-20), each time for 10 min. The rinsed PVDF membrane was immersed in the enhanced chemiluminescence (ECL) system solution to enhance the response signals, and the images were quantified with the Image Concentration analyzer. IL-6 was determined with IL-6 kits following the instructions of R & D System (Boston, USA).

Detection for the Expression of the Gene *hif-1α*. *RNA Extraction.* The embryos (HH stage 28) frozen at −80 °C were removed. To the tissue embryo (100 mg), 1 mL of TriReagent (Sigma, Co., Poole, England) was added and homogenized. The homogenate was left at ambient temperature for 5 min to facilitate the separation of nucleoproteins. The mixture, after 0.2 mL of chloroform was added and agitated vigorously for 15 s at ambient temperature for 2−3 min,

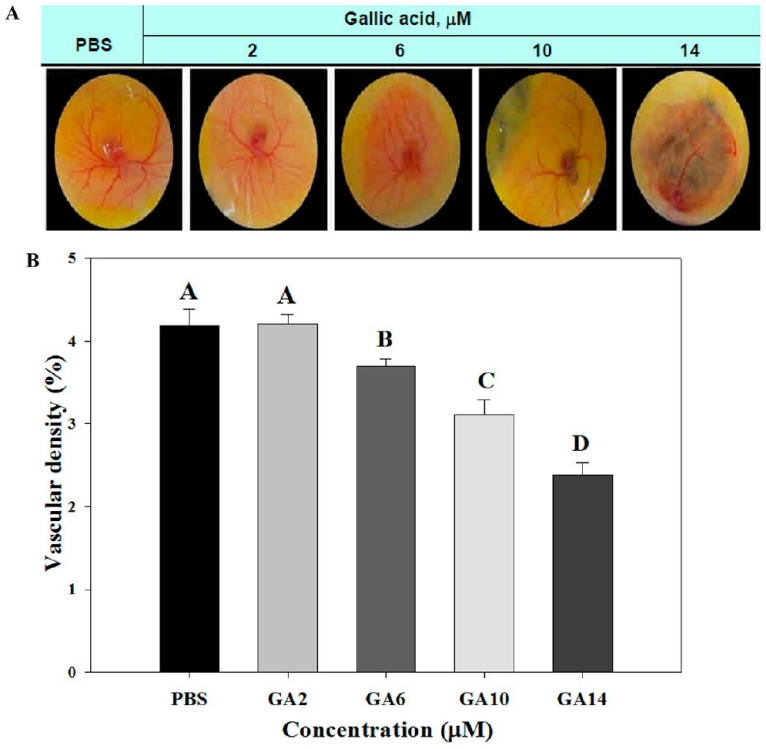

C Scoring for the pathological changes of cervical muscles in day-1 chicks.

Score	0	1	2	3	4
Appearance of cervical muscles	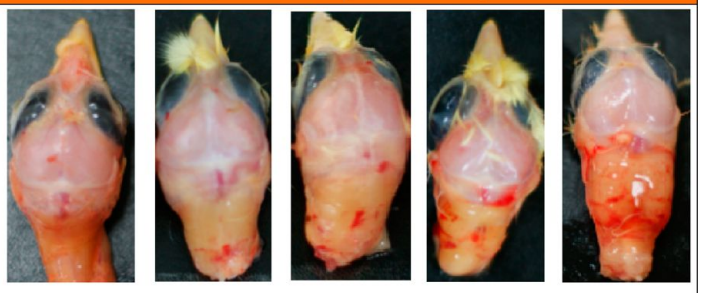				
Description of the status	Normal	Slight degree of hemolysis with liposis	Moderate hemolysis with liposis	Sub-degree hemolysis with liposis	Severe hemolysis with liposis

Figure 1. *In vivo* vascularization of day 5.5 embryos in the chicken embryo model (CEM) affected by gallic acid. Status of dysvascularization affected by gallic acid in a dose-dependent manner (A). Quantification of the vascularization (B) and the scoring for the pathological changes of cervical muscles in day-1 chicks (C).

was centrifuged at 4 °C and 12000*g* for 15 min. At this time, the upper layer of the mixture would look yellow (the phenol chloroform layer containing the RNA, approximately 0.6 mL per mL of TriReagent), and then there would be a middle layer and a colorless aqueous layer. The upper layer was sucked out carefully with a microcentrifuge tube and transferred into a new centrifuge tube. To the separated upper layer, 0.25 mL of isopropanol and 0.25 mL of polysaccharides (PS) proteoglycans (PG) removal solution were added, mixed well, left at ambient temperature for 10 min, and then centrifuged at 4 °C and 12000*g* for 10 min. The supernatant was discarded. To the TriReagent (Sigma, Co., Poole, England), 1 mL of ethanol (75%) was added to rinse the RNA pellet. The rinsing was repeated twice. The residue was mixed well and centrifuged at 4 °C and 12000*g* for 5 min. The ethanol was removed. The RNA pellet was desiccated at ambient temperature for 5−10 min with blown nitrogen. The RNA pellets were redissolved in 25 μL of double distilled water (dd water) previously treated with diethylpyrocarbonate (DEPC). The optical density was measured with Nano-Drop 1000 spectrophotometer (Thermo Fisher Scientific Inc., Waltham, MA, USA). The ratio A_{260}/A_{280} was calculated. This ratio must be within the range 1.7−1.9. The concentration of RNA was calculated, and the RNA preparation was stored at −80 °C for further use.

Reverse Transcription Polymerase Chain Reaction. To 4.5 μL of RNA obtained as described the above, 4.5 μLof oligo dT primer, 1 μL of random primer, and 1 μL of DEPC water were added to make a final volume of 10 μL. The mixture was heated in a dry bath heater at 70 °C for 5 min and then immediately cooled in ice chips for 3 min. To the mixture, 2 μL of 10 × MMLV buffer, 1 μL of 10 mM dNTP, 1 μL of MMLV reverse trancriptase, and 5 μL of DEPC-treated water were added to obtain a final volume of 20 μL. The mixture was placed in the PCR incubator at 37 °C for 4 h, changed to 85 °C for 5 min, then at ambient temperature for 24 h. The OD ratio was measured (preferably between 1.7 and 2.0). The cDNA obtained was diluted to 300 ng/μL and stored at −20 °C for use.

Polymerase Chain Reaction (PCR) to Detect the Gene *hif-1α*. To identify the expression of the gene *hif-1α* and the reference gene

dx.doi.org/10.1021/tx300456t | *Chem. Res. Toxicol.* 2013, 26, 325−335

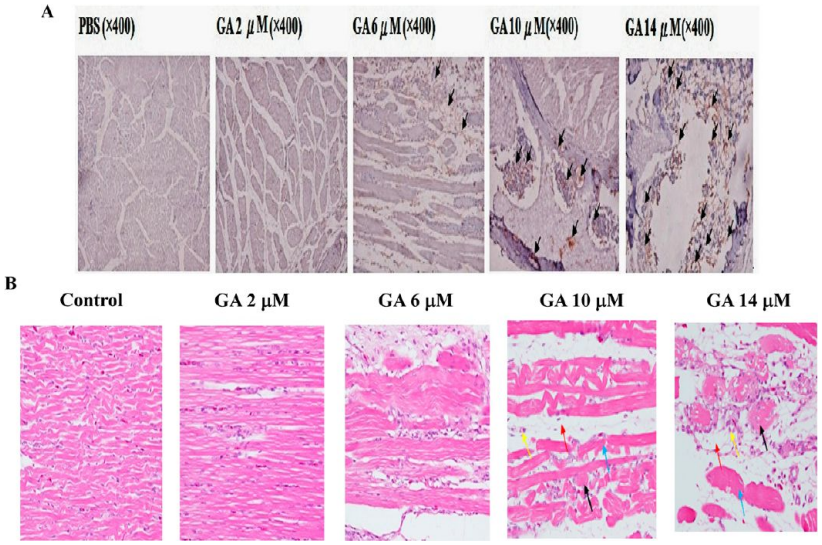

Figure 2. Immunohistochemical stain of tissue TNF-α and Hematoxylin−Eosin stain of cervical muscles obtained from day-1 chicks in CEM affected by gallic acid. The IHC staining revealed the tissue TNF-α to be expressed by gallic acid in a dose-responsive manner (A) (magnification: ×400). Cervical muscles were severely damaged by GA in a dose-responsive manner (B) (magnification: ×400). Black arrows: inflammation. Blue arrows: muscle defect. Yellow arrows: neutrophil accumulation. Red arrows: edema.

gapdh in the HH stage 28 chicken embryos, Gene Maker PCR Kit (Gene Marker, Taichung, Taiwan) was used. Briefly, 3 μL of cDNA (300 ng/μL), 1 μL of GeneTaq polymerase, 2.5 μL of GeneTaq buffer, forward 0.75 μL of primer (5 μM), 0.75 μL of reverse primer (5 μM), 15.5 μL of dd water, and 1.5 μL of dNTP were mixed to obtain a final volume of 25 μL. The mixture was used to carry out the PCR. The conditions used were predenaturation at 94 °C for 3 min, denaturation at 94 °C for 30 s, annealing (gene *hif-1α*) at 52 °C for 30 s, (gene *gapdh*) at 53 °C for 30 s, extension at 72 °C for 45 s, final extension at 72 °C for 3 min, and finally cool down to 20 °C for 2 min. The forward and reverse primers of gene *hif-1α* were forward primer, (-TGACACGAGTAGTGCCC); and reverse primer, (-CTGCCCTA-GAAGTTTACTCG).

Agarose Electrophoresis for DNA. Agarose was weighed and mixed with 5 × TAE buffer to obtain a concentration of approximately 0.8−1.5% w/v. The mixture was heated in the microwave until completely dissolved. To the solution, 3 μL of the internal Safe View DNA stain/100 mL was added and mixed well. The mixture was cooled at ambient temperature for 10 min and then poured into the casting plate. At the same time, the gas bubbles generated in agarose were carefully eliminated. The casted agarose plate was cooled at ambient temperature avoiding direct sunlight until completely coagulated. The agarose plate was placed in the electrophoresis chamber using 5 × TAE buffer as the electrophoretic buffer solution. DNA (100 ng/μL), mixed well with 6× loading dye, was injected into the concave slit of the agarose plate. Then, 100 V of electricity was applied for 20 min. The pattern was automatically photographed using Luminescence/UV Image System and contrasted with the reference DNA ladder. The brightened bands were examined to see whether it had matched the reference position. The photos were taken and quantified.

***In Vitro* Polyphenolics Erythrocyte Model (PEM).** *Isolation of Erythrocytes from Normal Day-1 Chicks.* Normal day-1 chicks were euthanized, and 5 mL of the blood were transferred immediately into a serum bottle in which several glass beads had been previously placed. The serum bottle with blood was agitated for 10 min to separate the fibrinogens. The defibrinated blood was centrifuged at 1500*g* for 15 min to separate the supernatant serum. The serum was discarded. To 1 mL of the red blood cell (RBC) sediment, 40 mL of normal saline (0.92%, pH 7.4 ± 0.1) was added to rinse the RBC. The rinses were repeated three times. Each time, the erythrocytes were centrifuged by centrifugation at 1500*g* for 15 min. The RBC sediment was suspended to 2% with normal saline (0.92%, pH 7.4 ± 0.1) (erythrocyte suspension, ERS).

Tracking the in Vitro RBC Hemolysis. To each 0.1 mL of ERS, 5 mL of normal saline (0.92%, pH 7.4 ± 0.1) containing 2, 6, 10, and 14 μM gallic acid was added. The mixtures were agitated for a few seconds while being capped. One drop of this suspension was transferred with a microdropper to the microscopic glass slide. After gentle smearing with a fine glass rod, the morphology of RBC was observed under a light microscope at magnifications of ×40 and ×400. The observations were observed at intervals of 4 h and continued for a total period of 24 h.

Determination of the in Vitro Dissolved Oxygen Consumption. The dissolved oxygen (DO) was determined with a DO meter (Hach 2968800, USA). Briefly, each ERS (0.1 mL) was added to 5 mL of the isotonic saline (0.92%, pH 7.4) containing 0, 2, 6, 10, and 14 μM gallic acid. The mixture was agitated for a few seconds while being capped. The measurement of DO was conducted at 20 min intervals for a whole course of 180 min. Similarly, triplicate experiments were carried out. The data obtained were treated statistically.

Assay for the in Vitro Ferrous Ion Release. A similar protocol was carried out as indicated in the above section. To 100 μL of supernatant, 100 μL of *o*-phenanthroline reagent was added. The mixture was left to stand for 5−10 min to facilitate the reaction. The optical density was read at 500 nm. The measurement of Fe(II) ions was conducted at 3 h intervals for a whole course of 24 h. Triplicate experiments were carried out. The concentration of ferrous ions was calculated from the standard curve similarly established.

Assay for the in Vitro Ferric Ion Transformation. A similar protocol was carried out as indicated in the above section. An aliquot of 200 μL of the test solution was accurately measured and centrifuged at 1500*g* for 5 min. The supernatant was transferred into a microtube. To 100 μL of the supernatant, 100 μL of KSCN reagent was added. The mixture was left to stand for 5−10 min, and the optical density was taken at 480 nm. The measurement of Fe(III) ions was conducted at 3 h intervals for a whole course of 24 h. Triplicate experiments were carried out. The concentration of ferric ions was calculated from the reference curve similarly established using the standard iron powder (extra pure reagent grade, Wako Pure, Tokyo, Japan) dissolved in reagent grade HCl (Wako Pure, Tokyo, Japan).

Assay for the in Vitro Hydrogen Peroxide Production. The *in vitro* hydrogen peroxide production was determined using the fluorescent probe DCFH-DA.[12] Briefly, to each 5 mL of normal saline containing GA at 0, 2, 6, 10, and 14 μM, 0.1 mL of 10 μM ERS was added. The mixture was agitated for a few seconds while being capped. To each sample, 10 μM DCFH-DA (Beyotime Institute of Biotechnology,

dx.doi.org/10.1021/tx300456t | *Chem. Res. Toxicol.* 2013, 26, 325−335

China) was added and left to stand for 30 min avoiding direct sunlight. The chemifluorescence was measured at λ_{Ex} = 488 nm and λ_{Em} = 532 nm.[12] The determination of hydrogen peroxide was performed at 6 h intervals until 24 h. Standard hydrogen peroxide solution ranging from 0 to 800 μM was used for calibration. The experiments were repeated in triplicate. The data obtained were treated statistically.

Statistical Analysis. Data obtained were analyzed by ANOVA and Duncan's tests with Microsoft Excel and computer statistical SPSS (version 15.0) software (SPSS, Chicago, IL). The significance of difference was judged by a confidence level of $p < 0.05$.

RESULTS AND DISCUSSION

Gallic Acid Inhibited the Vascularization in Embryos. GA showed a rather distinct inhibitory effect on the vascularization in CEM (Figure 1A). Vascularization was inhibited by GA in a dose responsive manner (Figure 1B). GA at 2 μM did not show any detrimental effect. The malformation rate reached the optimal rate (37.4%) with reduced mortality rate (46.1%) at 10 μM, far better than those induced by 14 μM GA (not shown herein; corresponding data were 29.2% and 70.9%). GA at 6 μM, 10 μM, and 14 μM suppressed the vascularization to 3.60%, 3.05%, and 2.25%, respectively, comparing with the control 4.15%, corresponding to relative reductions of 13.25%, 26.5%, and 45.78%, respectively, similar to the data previously reported.[5]

Gallic Acid Damaged the Cervical Muscle of Day-1 Chicks. The GA treated embryos showed severe damaged cervical muscles, with characteristics of edema, inflammation, Zenker's necrosis, liposis, and hemolysis (Figure 1C); similar results were reported by Hsieh et al.[5] The scores of hemolysis plus liposis that each group obtained approximately were 0.0, 0.0, 1.4, 2.3, and 3.2 for the PBS control, 2 μM GA, 6 μM GA, 10 μM GA, and 14 μM GA, respectively.

Immunohistochemical Stain Revealed Highly Induced Tissue TNF-α. Tissue TNF-α was highly induced in the cervical muscles when treated with gallic acid (Figure 2). GA at 2 μM did not show any TNF-α activating effect. At 6 μM, slight upregulation of TNF-α occurred. A huge amount of cytosolic TNF-α was overexpressed at 10 μM. At 14 μM GA, the cytosolically produced TNF-α was seen mobilized toward the membrane surface, possibly to the TNF-α receptor (TNFR) sites. Eventually, the cells were severely enlarged and disrupted. Large vacuoles appeared as a consequence of edema and inflammation (Figure 2A). Apparent muscle damages were seen at doses 10 and 14 μM. The common symptoms found in the damaged cervical muscles were edema, inflammation, muscle defect, and neutrophil accumulation (Figure 2B).

Tissue Hypoxia Inducible Factor (HIF)-1α and Gene *hif-1α* Were All Upregulated. GA at 2 μM showed only a slight effect on the tissue HIF-1α level. At GA 6, 10, and 14 μM, HIF-1α was relatively raised from the control (1.00) to 2.56-, 2.98-, and 3.44-fold (Figure 3A), and simultaneous upregulation of gene *hif-1α* was observed (Figure 3B). Under hypoxic conditions, the HIF1-α accumulates and dimerizes with HIF1-β and translocates to the nucleus, where they interacts with cofactors such as CBP (CREB Binding Protein)/p300 and the Pol II (DNA polymerase II) complex to bind to HREs (hypoxia-responsive element) and activate the transcription of target genes.

HIF1-α also activates the transcription of NOS (nitric oxide synthase), which promotes angiogenesis and vasodilation.[13] Speculatively, the dysvacularization caused by GA may be more or less compensated in this way. Otherwise, overdilated vascular vessels potentially may elicit hemolysis.

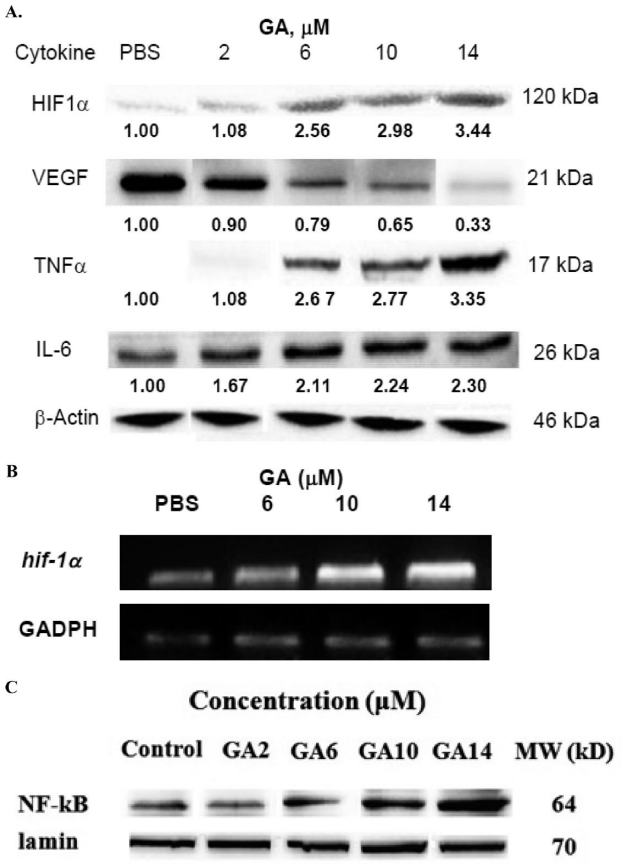

Figure 3. Expression of tissue proinflammatory cytokines and nuclear factor κB (NFκB) in the cervical muscles of day-1 chicks in CEM affected by gallic acid. The expression of tissue hypoxia inducible factor (HIF)-1α, VEGF, TNF-α, and IL-6 (A), *hif-1α* gene (B), and nuclear factor κB (NFκB) (C) in the cervical muscles of day-1 chicks after treatment with gallic acid at 2, 6, 10, and 14 μM, respectively.

VEGF Was Severely Downregulated by Gallic Acid. GA significantly downregulated the VEGF of cervical muscles in a dose-responsive manner (Figure 3A) to 0.90-, 0.79-, 0.65-, and 0.33-fold at 2, 6, 10, and 14 μM, respectively, strongly supporting the antiangiogenic and dysvascularizing effects of GA (Figure 1A and B). Literature elsewhere indicated that at a dose of 0.1% w/w i.p. GA caused 41% inhibition of angiogenesis.[4] Alternatively, hypoxic embryonic hearts showed increases in VEGF expression,[14] contradictory to the phenomena elicited in the cervical muscles.

HIF1-α-activated genes include VEGF, which promotes angiogenesis; GLUT1 (glucose transporter-1), which activates glucose transport; LDH (lactate dehydrogenase), which is involved in the glycolytic pathway; and Epo, which induces erythropoiesis.[13] Obviously, the VEGF-downregulating effect of GA has strongly supported the unique antiangiogenesis effect of GA in parallel to the upregulation of HIF-1α (Figure 3A), consistent with that cited.[4] Apparently, the hypoxic state in embryos can be greatly enhanced by downregulated vascularization.

The hypoxia-inducing effect of GA is seldom cited. *Rubia cordifolia* Linn. (Rubiaceae), enriched in GA at a level 1.8679 $\pm$ 0.29 μg/g (M-RC), significantly potentiated sodium nitrite-induced hypoxia and decreased the latency for death after sodium nitrite administration.[15] Hypoxia could cause decreased cardiac performance and cardiomyopathy in chick embryos,

dx.doi.org/10.1021/tx300456t | Chem. Res. Toxicol. 2013, 26, 325−335

involving a significant VEGF-mediated component.[14] Growth-restricted hypoxic chick embryos showed cardiomyopathy as evidenced by left ventricular (LV) dilatation, reduced ventricular wall mass, and increased apoptosis. This cardiomyopathy can persist into adulthood.[14]

Western Blot Also Revealed Highly Upregultated TNF-α and IL-6. Compared to HIF-1α, more prominent responses for TNF-α to 2.67-, 2.77-, and 3.55-fold and less responsive for IL-6 attaining only 2.11-, 2.24-, and 2.30-fold, respectively (Figure 3A), were observed. Collectively, GA acted likely as a strong hypoxia inducer as well as an inflammatory stress triggering factor in the cervical muscles of day-1 chicks. Literature elsewhere indicated that GA inhibited mast cell-derived inflammatory allergic reactions by blocking histamine release and pro-inflammatory cytokine (TNF-α and IL-6) expression.[16] Such an inhibitory effect is nuclear factor-κB (NFκB)- and p38 mitogen-activated protein kinase (p38 MAPK)-dependent.[16] Conversely, we suggest that the inflammation-inducing mechanism by GA in the cervical muscles of chicken embryos was due to the hypoxic state created by the prooxidant bioactivity of GA, which deprived most of the oxygen, resulting in inflammation, focal cell infiltration, liposis, and Zenker's necrosis of the cervical muscles.[5]

Nuclear Factor Kappa B (NFκB) Was Highly Upregulated. The activation of NFκB is closely related to oxidative stress. Activation of NFκB stimulates the production of inflammatory proteins such as TNF-α and interleukin-1β (IL-1β), which in turn activate the expression of MAPK. Such a synergistic cycling effect may greatly enhance the production of ROS and exert more severe damage to endothelial cells.[17]

There are three signaling pathways leading to the activation of NFκB known as the canonical pathway (or classical), the noncanonical pathway (or alternative pathway), and the atypical pathway.[18−22] In the canonical pathway, TNF-α, IL-1, and LPS are the common ligands, which activate the formation of (NEMO)·(IKKα)·(IKKβ) and the p50·[(RelA)·(RelA)]·(pp-IκB)] complexes. Subsequently after cascade transformation, NFκB was activated. Alternatively, the atypical pathway can be divided into two subpathways: the IKK-dependent and the IKK-independent pathways. In the IKK-independent atypical pathway, tyrosine kinase (TRK) is activated by hypoxia and hydrogen peroxide; otherwise, CK2 is triggered by UV and HER2·Neu to produce complex [(RelA)·(RelA)·(pp-IκBα)·(p-50)]. The dissociation of I$\kappa\alpha$ from the TRK pathway or the degradation of I$\kappa\alpha$ in both the TRK and the CK2 paths will yield the complex [(RelA)·(RelA)·(p50)]. The latter is translocalized into the nucleus, and after a cascade of reactions, NFκB is activated. In the IKK-dependent atypical pathway, NEMO is separately activated to form the (NEMO)·(ATN)(Sumo) complex, which on ubiquitylation en route to the canonical pathway proceeds as in the above-mentioned case. The NFκB was upregulated by GA at a dose $\geq$6 μM in a dose-dependent manner reaching 1.44-, 1.98-, and 2.98-fold compared to the PBS control, when, respectively, administered 6, 10, and 14 μM GA (Figure 3C). In all pathways exclusive of the noncanonical pathway, the activation of NFκB eventually leads to the transcriptional events affecting survival, proliferation, inflammation, and immune regulation, while the noncanonical pathway independently leads to lymphogenesis and B cell maturation. The simultaneous upregulation of TNF-α, IL-1, and HIF-1α and the downregulation of VEGF indicated that the action mechanism exerted by GA could be very complicated. Speculatively, hypoxia and hydrogen peroxide might take the path en route to the IKK-independent atypical pathway, while TNF-α and IL-6 might take the canonical pathway. Alternatively, the upregulation of the *hif-1α* gene (Figure 3C), a genotoxic stress, might activate the IKK-dependent atypical pathway. To further understand why in the *in vivo* model gallic acid could have induced such a unique *in vivo* hypoxic state and hemolysis symptoms, we conducted the following *in vitro* experiments.

***In Vitro* Disruption of Erythrocytes Induced by Gallic Acid.** In the isotonic physiological saline, GA induced RBC swelling and disruption. The extent of cell swelling and rupture seemed to be in a dose- and time-dependent manner (Figure 4). Within a period shorter than 3 h, there still did not seem to be any hemolytic event occurring. At 6 h, only the RBCs treated with 10 μM and 14 μM GA started to disrupt. When disrupted, the nuclei were released, leaving the RBC sacs suspended like swollen reddish balloons in the normal saline (Figure 4). A longer time was required for the lower GA

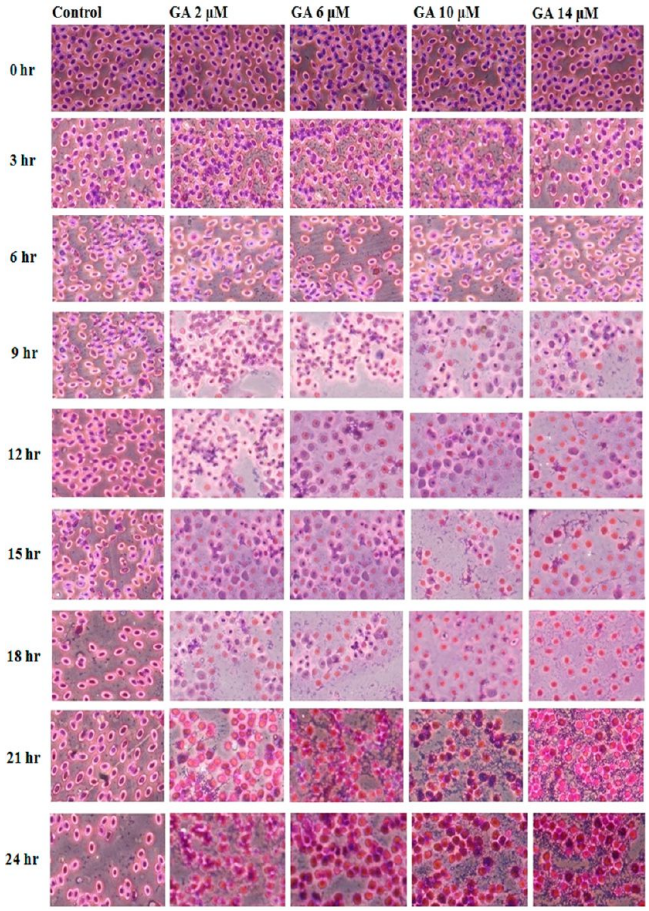

Figure 4. *In vitro* polyphenolics erythrocyte model (PEM) to explore the supporting action mechanism(s) of hemolysis induced by gallic acid. Chicken erythrocytes were tested for hemolytic behavior in the presence of gallic acid at 0 (normal saline control, 0.92% NaCl solution, pH. 7.4), 2, 6, 10, and 14 μM at ambient temperature for a whole course of 24 h. Each observation was set at intervals of 3 h. Magnification: ×400. As seen, the Fe^{2+} ions may be released with a two-phase kinetic mechanism. Supposedly at the initial stage (within a time $\leq$6 h), it could be triggered by the attack of semiquinones and quinones on the RBC cell membrane to form the C2 and C6 addition adduct(s). At the second stage (t > 6 h), a huge amount of Fe^{2+} ions would be released due to RBC rupture.

dx.doi.org/10.1021/tx300456t | *Chem. Res. Toxicol.* 2013, 26, 325−335

concentrations (2 μM and 6 μM) to disrupt the RBC. Complete disintegration of RBC only occurred until 24 h (Figure 4).

***In Vitro* Dissolved Oxygen Was Rapidly Depleted by Gallic Acid.** We performed this *in vitro* experiment in a closed system where no free atmospheric oxygen was allowed to leak in to mimic the dissolved oxygen (DO) depletion. GA actually was shown to have consumed DO *in vitro* in both a time- and a dose-dependent manner (Figure 5). The depletion of DO was

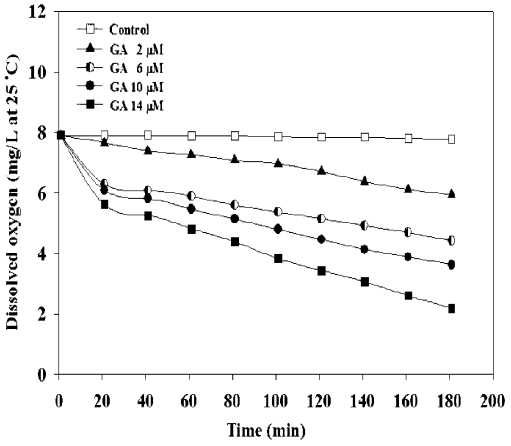

Figure 5. Time- and dose-dependent depletion of dissolved oxygen affected by gallic acid in *in vitro* PEM. As DO < 5 ppm is lethal to the aerobes, the depletion can be considered completed within 3 h by a GA dose at ≥6 μM.

completed shortly within 3 h, implying that the role of DO could have been active only in the initial phase to accelerate the formation of semiquinones and quinones.[8]

At a normal arterial oxygen partial pressure of 100 mmHg, only 0.003 mL of oxygen is dissolved per milliliter of blood. As a result, only 0.30 mL (0.31 vol%) of O_2 is carried in solution in each 100 mL of arterial blood at normal arterial blood oxygen tension (PaO_2) and normal body temperature, which is a very small amount compared to the gallic acid concentration administered. Hence, the gallic acid in plasma is able to deplete the dissolved oxygen in blood. However, once hemoglobin is fully saturated, further increases in oxygen partial pressure can affect only the plasma dissolved oxygen fraction.[23]

Release of Ferrous Ions from the Erythrocytes Distinctly Revealed a Two-Phase Mechanism, Which Coincided with the Oxygen Depletion by Gallic Acid. The ferrous ion release from the deformed erythrocytes and the transformation of ferrous to ferric ions all distinctly showed a two-phase mechanism (Figure 6). The dividing point was approximately at 12 h (Figure 6). Such a two-phase mechanism phenomenon closely coincided with the depletion of oxygen by GA (Figure 5).

However, due to the limited catalytic effect exerted by the Haber–Weiss reaction, the formation of ferric ions remained only in trace amount. Autooxidation of GA increases radical intensity and changes the redox potential to a more oxidative state,[24,25] leading to tremendous formation of semiquinone and superoxide ($\cdot O_2^-$) radicals.[26,27] Hence, part of the hemolytic effect in embryos could be induced by the autoxidative behavior of GA, whereby huge amounts of reactive oxygen species can be generated.[3] Both the superoxide ($\cdot O-^-$) and the hydroxyl

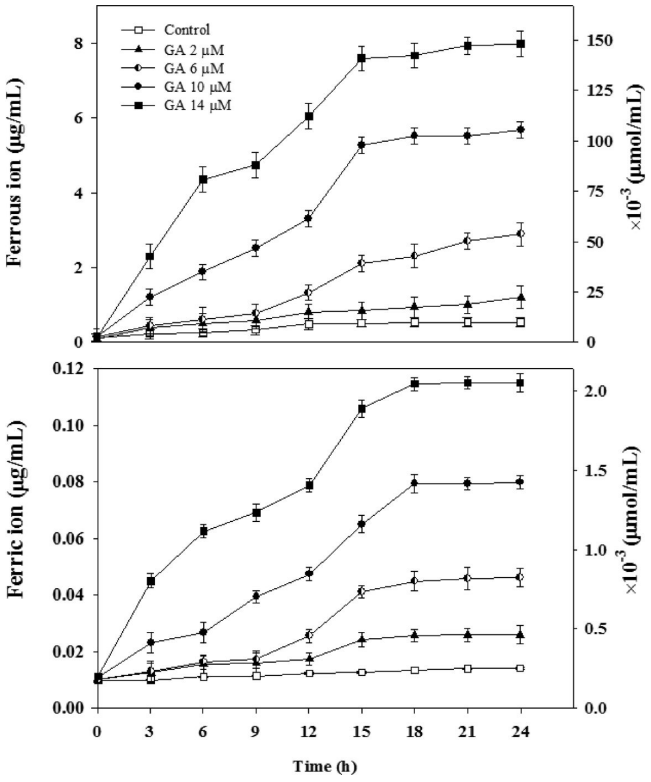

Figure 6. Two-phase kinetic pattern related to the release of ferrous ions (upper panel) from erythrocytes treated with gallic acid and its transformation into ferric ions (lower panel) in *in vitro* PEM. The two-phase kinetics apparently implicated two different RBC-damaging mechanisms.

radicals can accelerate autoxidation to generate H_2O_2.[28] As mentioned above, the depletion of membrane sulfhydryl groups and the C2–C6 peptide addition reactions could alter the membrane permeability, contributing to the initial release of ferrous ions from the erythrocytes (in the form of hemoglobin-Fe^{2+}), even though the erythrocytes were not ruptured (Figure 7). The information of the present study may provide fresh

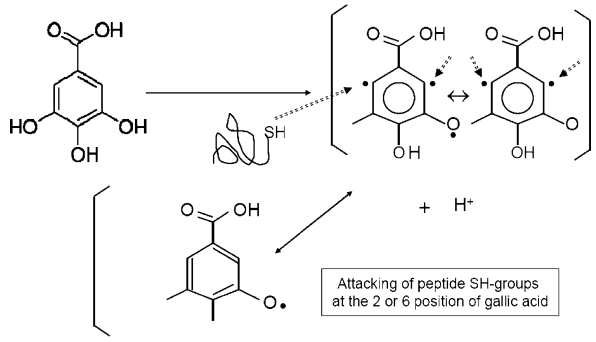

Figure 7. Schematic presentation of the 2,6-attack by peptides on gallic acid nuclear bezoyl structure.

insight into the prooxidant effect and cytotoxicity of the gallyl moiety containing phytochemicals.[29] Interestingly, GA is able to inhibit gap-junction intercellular communication (GJIC; a carcinogenic phenomenon).[30] Thus, we speculate that within the blood pH value 7.3 to 7.5, GA can be more rapidly oxidized in some organs that are actively transporting oxygen, such as lungs, erythrocytes, and bone marrow. In developing embryos,

dx.doi.org/10.1021/tx300456t | *Chem. Res. Toxicol.* 2013, 26, 325–335

the endothelial membrane, the angiogenic system, and the red blood cells would be actively developing and differentiating in many tissues such as nerves, internal organs, and blood vessels, underlying the target organs of GA cytotoxicity during the embryonic developments.

Kinetic Analyses on the *in Vitro* Ferrous Ion Release from Erythrocytes Induced by Gallic Acid. As shown, the erythrocytes released ferrous ions in a time- and dose-responsive manner in the presence of GA (Figure 6). Assuming the release rate to obey the first order kinetic, e.g., for GA = 14 μM, we have

$$\text{Rate} = dC/dt = k_{(II),14}[C] \quad (1)$$

Substitution of the experimental data obtained in Figure 6, i.e., $dC \approx \Delta C = 130 \times 10^{-3}$ μmol·mL^{-1}, $dt \approx \Delta t = 12$ h, and [C] = 0.014 μmol·mL^{-1} (for GA at 14 μM), leads to

$$dC/dt = (130 \times 10^{-3}\ \mu\text{mol·mL}^{-1}/12\ \text{h}) = 10.83 \times 10^{-3}\ \mu\text{mol·mL}^{-1}\text{·h}^{-1} \quad (2)$$

and from eq 1, we had

$$10.83 \times 10^{-3}\ \mu\text{mol·h}^{-1}\text{·mL}^{-1} = k[0.014\ \mu\text{mol·mL}^{-1}] \quad (3)$$

or

$$k_{(II),4} = 0.774\ \text{h}^{-1} \quad (4)$$

Similarly, for the GA at 10 μM and 6 μM

$$k_{(II),10} = 0.525\ \text{h}^{-1} \quad (5)$$

and

$$k_{(II),6} = 0.347\ \text{h}^{-1} \quad (6)$$

Assuming the first kinetic order also to be applicable to the formation of ferric ions, Fe(III), similar treatment led to the formation rate coefficients of Fe(III): for GA at 14 μM, 10 μM, and 6 μM to be $k_{(III),14} = 8.93 \times 10^{-3}$ h^{-1}, $k_{(III),10} = 6.66 \times 10^{-3}$ h^{-1}, and $k_{(III),6} = 6.66 \times 10^{-3}$ h^{-1}, respectively. In contrast, the prooxidant activity of GA has been reported to be 0.0090 min^{-1}, being comparable to the highest 0.0091 min^{-1} of EGCG.[31] Thus, the formation rate coefficients of ferric ions were very low, reaching only about one thousandth that of ferrous ions. Hence, as speculated, the initial depletion of DO might be used only to induce the formation of semiquinones and quinones from GA,[26,27] causing the accelerated autoxidation of GA in phase I (Figures 4 and 5),[3,28] while most of the ferrous and ferric ions produced in phase II could be resulting from the altered membrane permeability or disruption of RBC (Figure 6).

GA has been shown to increase radical intensity and change the redox potential to a more oxidative state.[24,25] In the Haber–Weiss reactions (eqs 2–4), iron is involved in free radical production (eqs 2–4).[32] In the presence of Fe(II) or Fe(III) ions, ROS is produced by two coupled reactions: the Haber–Weiss reaction (eqs 7–9) and the Fenton reaction (eq 10):[32]

$$Fe^{2+} + O_2 \leftrightarrows Fe^{3+} + \cdot O_2^- \quad (7)$$

$$\cdot O_2^- + 2H^+ \rightarrow H_2O_2 + O_2 \quad (8)$$

$$Fe^{3+} + \cdot O_2^- \rightarrow Fe^{2+} + O_2 \quad (9)$$

$$Fe^{2+} + H_2O_2 \rightarrow Fe^{3+} + OH^- + \cdot OH \quad (10)$$

Simultaneously, other cyclic autoxidations may occur, however, only with minute contributions:

$$H_2O_2 + \cdot OH \rightarrow H_2O + \cdot O_2^- + H^+ \quad (11)$$

$$H_2O_2 + \cdot O_2^- \rightarrow O_2 + OH^- + \cdot OH \quad (12)$$

The detailed mechanism responsible for this effect of GA has not been elucidated. Otherwise, the value of pH could alter the chemical activity of GA, more pronounced in the pH region 6–12.[33,8] These reactions (eqs 7–10) in reality are actually occurring *in vivo* and *in vitro*, achieving notoriety as a possible source for oxidative stress. In developing embryos, the proliferation of the smooth muscle membrane is intensively differentiating in many developing tissues such as nervous tissue, internal organs, and blood vessels, pointing to the targets of GA cytotoxicity in these developing organs.

***In Vitro* Gallic Acid Induced Hydrogen Peroxide Obeyed Two-Phase Kinetics.** The *in vitro* production of hydrogen peroxide also distinctly revealed a two-phase pattern. Phase I started from h0 to h12, and phase II from h12 to h24 (Figure 8A). Assuming the first order kinetic to be applicable, phase I was shown to exhibit kinetic coefficients for GA at 14 μM, 10 μM, and 6 μM; $k_{(I)14\ \mu M} = 0.774$ h^{-1}, $k_{(I)10\ \mu M} = 0.292$ h^{-1}, and $k_{(I)6\ \mu M} = 0.236$ h^{-1}. In contrast, phase II exhibited larger kinetic coefficients such as $k_{(II)14\ \mu M} = 2.560$ h^{-1}, $k_{(II)10\ \mu M} = 2.460$ h^{-1}, and $k_{(II)6\ \mu M} = 0.764$ h^{-1}, corresponding to the

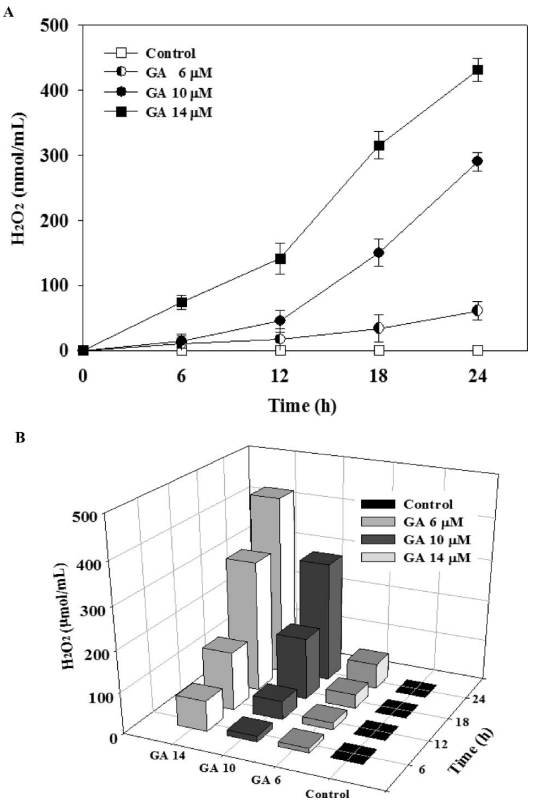

Figure 8. Hydrogen peroxide production affected by GA in *in vitro* PEM. The hydrogen peroxide concentration–time (C_{H2O2}-t) curve showing a two-phase pattern (A). The 3D-overall result of the hydrogen peroxide concentration–time (C_{H2O2}-t), the GA dose–hydrogen peroxide concentration (C_{GA}-C_{H2O2}), and the GA dose–time relationship (C_{GA}-t) (B).

dx.doi.org/10.1021/tx300456t | *Chem. Res. Toxicol.* 2013, 26, 325–335

increase of 3.31-, 8.43-, and 3.24-fold, respectively. Apparently, the sharp increase in phase II could be relevantly related to the huge amount of ferrous ion release from the erythrocytes. Alternatively, the production of hydrogen peroxide due to the increased ferrous ion release was dose-dependent on GA (Figure 8A). The Fe(II) ions catalyzed the production of hydrogen peroxide through the Haber–Weiss reaction.[32] The 3D overall results of the hydrogen peroxide concentration–time (C_{H2O2}-t), the GA dose–hydrogen peroxide concentration (C_{GA}-C_{H2O2}), and the GA dose–time relationship (C_{GA}-t) are shown in Figure 8B.

In a cell-free system, GA produced ·OH in the presence of Fe^{2+}-EDTA, which was quenched by catalase, suggesting the involvement of the Haber–Weiss reaction.[3] The production of hydrogen peroxide was consistent with the release kinetic of ferrous ions from the RBC (Figures 6 and 8). In general, the toxicity of iron often has been attributed to its ability to reduce molecular oxygen, thus forming partially reduced oxygen species.[34]

Literature elsewhere indicated that GA failed to protect against H_2O_2-induced PC12 cell death, which was ascribed to the prooxidant potential and generation of ROS by GA.[26,27,35] GA at concentrations up to 12 μM could not inhibit the peroxidation of phospholipids in the liposomal system.[36] In contrast, some antioxidants such as ascorbic acid and *N*-acetylcysteine were shown to be effective in protecting other cell lines,[5] implicating different substrate-specific and cell–specific responses.

Thus, the close link of the *in vitro* and the *in vivo* data has now been verified. GA can be nonenzymatically oxidized *in vivo* physiological solutions (37 °C, pH 7.4) to produce superoxide anions, H_2O_2 and GA quinones.[33,8] In addition, GA tends to increase ROS levels including $\cdot O_2^-$ and induce GSH depletion. Furthermore, GA inhibited the growth of lung cancer and normal cells.[37] As mentioned, one of the most commonly accepted mechanisms by which iron is involved in free radical production is demonstrated by the iron-mediated Haber–Weiss reactions (eqs 2–4).[32] In the presence of Fe(II) or Fe(III) ions, the *in vivo* ROS would be rapidly produced by two coupled reactions: the Haber–Weiss with the Fenton reaction.[32]

Literature also indicated that GA dose-dependently generated considerably more H_2O_2 in DMEM media without cells than did quercetin, indicating GA to have stronger antiproliferative activity than quercetin.[30] Both $\cdot O_2^-$ and ·OH radicals could accelerate autoxidation.[28] Moreover, the produced $\cdot O_2^-$ and ·OH radicals are very reactive and may damage major biomacromolecules such as proteins or DNA and consequently may induce teratogenicity or malformation. Interestingly, Lee et al. demonstrated that GA (but not quercetin) uniquely inhibited gap-junction intercellular communication (GJIC; a carcinogenic phenomenon).[30]

Since the disintegration of RBC did not start before h 3 (Figure 4), the hydrogen peroxide (HPO) level at h 3 only had reached 10 to 35 nmol/mL (or μM) at GA dose 6–14 μM (Figure 7A), while the safety normal level for HPO had been shown to be 40 μM,[38] we suggest that the initial release of ferrous ions (in the form of hemoglobin-Fe^{2+}) from RBC is likely to be caused by an alternate mechanism, i.e., the alteration of the membrane permeability. Chen et al. demonstrated that the catechol type quinones act as cross-linkers on which peptide chains may combine through thiol-S-alkylation at the C2- and C6-sites of the gallyl ring.[29] As a rule, a structure with a gallyl moiety is a prerequisite to induce the aggregation of membrane proteins and to deplete membrane sulfhydryls.[29] The depletion of such membrane sufhydryl groups can distort or ultimately disrupt the RBC membranes, resulting in huge amount ferrous ion release from BRC.

A summarized flowchart is shown in Figure 9, which demonstrates the link between the *in vitro* action mechanisms

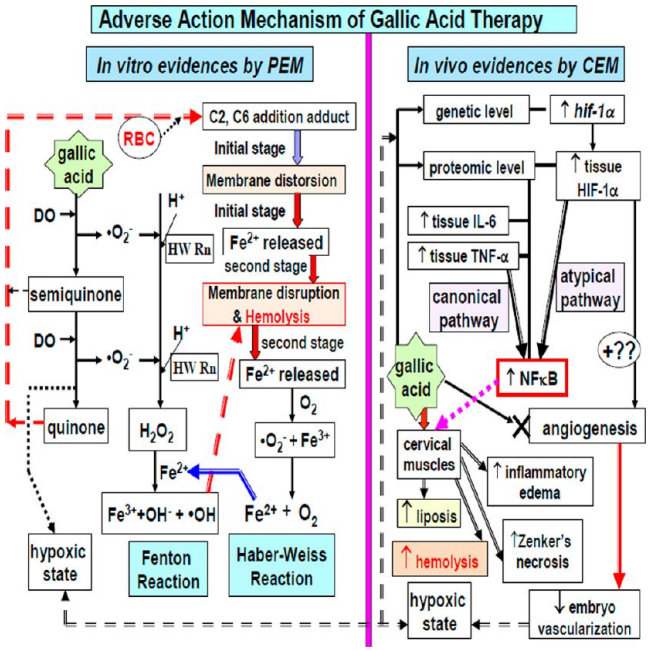

Figure 9. Linking of the evidence found in the *in vivo* CEM and the *in vitro* PEM to support the hemolytic and teratogenic action mechanism(s) of gallic acid. The prooxidant activity of GA depletes the DO and produces a huge amount of superoxide anions ($\cdot O_2^-$), which are transformed into H_2O_2 through the Haber–Weiss reaction and then to Fe^{3+}, OH^-, and ·OH ions by the catalytic Fe^{2+} ions (Fenton reaction). In addition, $\cdot O_2^-$ + Fe^{3+} are transformed into O_2 + Fe^{2+} (Haber–Weiss reaction). All of these reactions synergistically contributed to RBC hemolysis. In addition, the overexpression of NFκB in CEM may be triggered by the upregulated tissue TNF-α en route to the canonical pathway and by the upregulation of the gene *hif-1α*, through an atypical pathway, resulting in hypoxic inflammation and hemolysis.

of PEM and the *in vivo* findings in CEM. Briefly, gallic acid consumes dissolved oxygen (DO) to produce superoxide anions ($\cdot O_2^-$) and hydrogen peroxide through the Haber–Weiss reaction, resulting in a hypoxic state. For compensation, GA is in turn converted into semiquinones and quinines, the latter tend to form C2,C6 addition adducts with the membrane peptides, resulting in alteration of permeability or disruption of RBC. As a consequence, huge amounts of Fe^{2+} ions leak out after being attacked by semiquinones and quinones of gallic acid, which catalyze oxygen molecules to produce $\cdot O_2^-$ anions and hydrogen peroxide (HPO) (Haber–Weiss reaction). HPO was subsequently split into hydroxyl free radicals and hydroxide ions (Fenton reaction), enhancing the attack on RBC. This suggests that the teratogenicity of gallic acid may have resulted from the overexpression of NFκB that is activated by upregulated tissue TNF-α en route to the canonical pathway and the upregulation of the gene *hif-1α*, HIF-1α, and HPO through an atypical pathway. In addition, the Fenton and Haber–Weiss reactions initiated by the prooxidant activity of gallic acid are involved in the disruption of erythrocytes

dx.doi.org/10.1021/tx300456t | *Chem. Res. Toxicol.* 2013, 26, 325–335

resulting in hemolysis. Thus, the *in vitro* evidence obtained from the PEM have substantially supported the findings obtained from the *in vivo* CEM (Figure 9).

CONCLUSIONS

Gallic acid (GA) tends to elicit erythrocyte hemolysis despite *in vivo* CEM and *in vitro* PEM. In CEM, TNF-α, the gene *hif-1α*, HIF1-α, and NFκB are upregulated and VEGF downregulated. Usually, the cervical muscles are severely damaged, showing inflammatory edema, Zenker's necrosis, liposis, and hemolysis. In PEM, GA attacks the innate erythrocytes by a two-phase model, depleting all the dissolved oxygen (DO), deforming the erythrocyte membrane to evoke Fe(II) ions release and a hypoxic state. Fe(II) ions catalyze the generation of superoxide through the Haber−Weiss reaction, while phase II through the Fenton reaction produces huge amounts of ·OH radicals to induce RBC hemolysis.

AUTHOR INFORMATION

Corresponding Authors

*(K.C.C.) Tel: +886-2-22490088 ext. 8112. E-mail: kc.chen416@msa.hinet.net.

*(C.L.H.) Tel: +886-4-7232105 ext. 3452. E-mail: clhseih@cc.ncue.edu.tw.

*(R.Y.P.) Tel: +886-2-27585767. E-mail: ypeng@seed.net.tw.

Author Contributions

○Y.-B.K. and C.-C.P. contributed equally to this work.

Funding

This work was supported by the National Science Council [NSC 99-2313-B-018-002-MY3, 99-2320-B-038-011-MY3, 101-2320-B-039-040] and Taipei Medical University [TMU101-AE1-B11].

Notes

The authors declare no competing financial interest.

ABBREVIATIONS

CEM, chicken embryo model; GA, gallic acid; HIF-1α, hypoxia inducible factor; TNF-α, tumor necrosis factor-α; IL-6, interleukin-6; NFκB, nuclear factor kappa; VEGF, vascular endothelial growth factor; DO, dissolved oxygen; ROS, reactive oxygen species; PEM, polyphenolics erythrocyte model; HPO, hydrogen peroxide; VSMCs, vascular smooth muscle cells; HUVECs, human umbilical vein endothelial cells; HH stage, Hamburger and Hamilton stage; ECL, enhanced chemiluminescence; PVDF, polyvinylidene fluoride; PS, polysaccharides; PG, proteoglycans; DEPC, diethylpyrocarbonate; NOS, nitric oxide synthase; GLUT1, glucose transporter-1; LDH, lactate dehydrogenase; GJIC, gap-junction intercellular communication

REFERENCES

(1) Niemets, R., and Gross, G. G. (2005) Enzymology of gallotannin and ellgitannin biosynthesis. *Phytochemistry 66*, 2001−2011.

(2) Park, W., and Kim, S. H. (2012) Involvement of reactive oxygen species and glutathione in gallic acid-induced human umbilical vein endothelia cell death. *Oncol. Rep. 28*, 695−700.

(3) Qiu, X., Takemura, G., Koshiji, M., Hayakawa, Y., Kanoh, M., Maruyama, R., Ohno, Y., Minatoguchi, S., Akao, S., Fukuda, K., Fujiwara, T., and Fujiwara, H. (2000) Gallic acid induces vascular smooth muscle cell death via hydroxyl radical production. *Heart Vessels 15*, 90−99.

(4) Liu, Z., Schwimer, J., Liu, D., Lewis, J., Greenway, F. L., York, D. A., and Woltering, E. A. (2006) Gallic acid is partially responsible for the antiangiogenic activities of Rubus leaf extract. *Phytother. Res. 20*, 806−813.

(5) Hsieh, C. L., Wang, H. E., Tsai, W. J., Peng, C. C., and Peng, R. Y. (2012) Multiple point action mechanism of valproic acid-teratogenicity alleviated by folic acid, vitamin C, And N-acetylcysteine in chicken embryo model. *Toxicology 291*, 32−42.

(6) Strlic, M., Radovic, T., Kolar, J., and Pihlar, B. (2002) Anti-and prooxidative properties of gallic acid in Fenton-type system. *J. Agric. Food Chem. 50*, 6313−6317.

(7) Sakagami, H., and Satoh, K. (1997) Prooxidants: ascorbic acid and gallic acid. *Anticancer Res. 17*, 221−224.

(8) Gil-Longo, J., and González-Vázquez, C. (2010) Vascular pro-oxidant effects secondary to the autoxidation of gallic acid in rat aorta. *J. Nutr. Biochem. 21*, 304−309.

(9) Park, W., Chang, M. S., Kim, H., Choi, H. Y., Yang, W. M., Kim, do R., Park, E. H., and Park, S. K. (2008) Cytotoxic effect of gallic acid on testicular cell lines with increasing H_2O_2 level in GC-1 spg cells. *Toxicol. in Vitro 22*, 159−163.

(10) Hamburger, V., and Hamilton, H. L. (1992) A series of normal stages in the development of the chick embryo. 1951. *Dev. Dyn. 1992* (195), 231−72.

(11) Latacha, K. S., and Rosenquist, T. H. (2005) Homocysteine inhibits extra-embryonic vascular development in the chick embryo. *Dev. Dyn. 234*, 323−331.

(12) Nakajima, Y., Nishida, H., Nakamura, Y., and Konishi, T. (2009) Prevention of hydrogen peroxide-induced oxidative stress in PC12 cells by 3,4-dihydroxybenzalacetone isolated from Chaga (*Inonotus obliquus* (persoon) Pilat). *Free Radical Biol. Med. 47*, 1154−1161.

(13) Damert, A., Ikeda, E., and Risau, W. (1997) Activator-protein-1 binding potentiates the hypoxia-inducible factor-1-mediated hypoxia-induced transcriptional activation of vascular-endothelial growth factor expression in C6 glioma cells. *Biochem. J. 327*, 419−423.

(14) Tintu, A., Rouwet, E., Verlohren, S., Brinkmann, J., Ahmad, S., Crispi, F., van Bilsen, M., Carmeliet, P., Staff, A. C., Tjwa, M., Cetin, I., Gratacos, E., Hernandez-Andrade, E., Hofstra, L., Jacobs, M., Lamers, W. H., Morano, I., Safak, E., Ahmed, A., and le Noble, F. (2009) Hypoxia induces dilated cardiomyopathy in the chick embryo: Mechanism, intervention, and long-term consequences. *PLoS ONE 4* (e5155), 1−11.

(15) Patil, R., Gadakh, R., Gound, H., and Kasture, S. (2011) Antioxidative and anticholinergic activity of *Rubia cordifolia*. *Pharmacologyonline 2*, 272−278.

(16) Kim, S. H., Jun, C. D., Suk, K., Choi, B. J., Lim, H., Park, S., Lee, S. H., Shin, H. Y., Kim, D. K., and Shin, T. Y. (2006) Gallic acid inhibits histamine release and pro-inflammatory cytokine production in mast cells. *Toxicol. Sci. 91*, 123−131.

(17) Hsieh, C. L., Huang, C. N., and Peng, R. Y. (2007) Molecular action mechanism against apoptosis by aqueous extract from guava budding leaves elucidated with human umbilical vein endothelial cell (HUVEC) model. *J. Agric. Food Chem. 55*, 8523−8533.

(18) Karin, M. (1999) How NFkB is activated: the role of the IkB kinase (IKK) complex. *Oncogene 18*, 6867−6874.

(19) Tergaonkar, V. (2006) NFkB pathway: A good signaling paradigm and therapeutic target. *Int. J. Biochem. Cell Biol. 38*, 1647−1653.

(20) Gilmore, T. D. (2006) Introduction to NFkB: players, pathways, perspectives. *Oncogene 25*, 6680−6684.

(21) Scheidereit, C. (2006) IkB kinase complexes: gateways to NFkB activation and transcription. *Oncogene 25*, 6685−6705.

(22) Perkins, N. D. (2007) Integrating cell-signalling pathways with NF-kappaB and IKK function. *Nat. Rev. Mol. Cell Biol. 8*, 49−62.

(23) Calif International Congress on Hyperbaric Medicine (1984) Kindwall, E. P. In *Proceedings of the 8th International Congress on Hyperbaric Medicine*, August 20−22, 1984, Long Beach, CA (Hart, G. Ed.) Best Publishing Co., Palm Beach Gardens, FL.

(24) Severino, J. F., Goodman, B. A., Kay, C. W., Stolze, K., Tunega, D., Reichenauer, T. G., and Pirker, K. F. (2009) Free radicals generated during oxidation of green tea polyphenols: electron

paramagnetic resonance spectroscopy combined with density functional theory calculations. *Free Radical Biol. Med. 46*, 1076−1088.
(25) Bors, W., Michel, C., and Stettmeier, K. (2000) Electron paramagnetic resonance studies of radical species of proanthocyanidins and gallate esters. *Arch. Biochem. Biophys. 374*, 347−355.
(26) Wong, S. K., Sytnyk, W., and Wan, J. K. S. (1972) Electron spin resonance study of the selfdisproportionation of some semiquinone radicals in solution. *Can. J. Chem. 50*, 3052−3057.
(27) Eslami, A. C., Pasanphan, W., Wagner, B. A., and Buettner, G. R. (2010) Free radicals produced by the oxidation of gallic acid: An electron paramagnetic resonance study. *Chem. Cent. J. 4*, 15−18.
(28) Labieniec, M., and Gabryelak, T. (2006) Study of interactions between phenolic compounds and H_2O_2 or Cu(II) ions in B14 Chinese hamster cells. *Cell Biol. Int. 30*, 761−768.
(29) Chen, R., Wang, J. B., Zhang, X. Q., Ren, J., and Zeng, C. M. (2011) Green tea polyphenol epigallocatechin-3-gallate (EGCG) induced intermolecular cross-linking of membrane proteins. *Arch. Biochem. Biophys. 507*, 343−349.
(30) Lee, K. W., Hur, H. J., Lee, H. J., and Lee, C. Y. (2005) Antiproliferative effects of dietary phenolic substances and hydrogen peroxide. *J. Agric. Food Chem. 53*, 1990−1995.
(31) Tan,Y. Y., Quek,Y. L., and Huang, D. J. (2006) The Effect of Fermentation on Pro-Oxidant Activity of Tea Leaves, M.S. Thesis, National University of Singapore, Singapore.
(32) Kevin, D., Welch, T., Davis, Z., and Steven, D. (2002) Iron autoxidation and free Radical generation: effects of buffers, ligands, and chelators. *Arch. Biochem. Biophys. 397*, 360−369.
(33) Friedman, M., and Jürgens, H. S. (2000) Effect of pH on the stability of plant phenolic compounds. *J. Agric. Food. Chem. 48*, 2101−2110.
(34) Halliwell, B., and Gutteridge, J. M. C., Eds. (1984) (eds) In *Free Radicals in Biology and Medicine*, 2nd ed., Oxford University Press, New York.
(35) Simić, A., Manojlović, D., Šegan, D., and Todo, M. (2007) Electrochemical behavior and antioxidant and prooxidant activity of natural phenolics. *Molecules 12*, 2327−2340.
(36) Aruoma, O. I., Murcia, A., Butler, J., and Halliwell, B. (1993) Evaluation of the antioxidant and prooxidant actions of gallic acid and its derivatives. *J. Agric. Food Chem. 41*, 1880−1885.
(37) You, B. R, and Park, W. H. (2010) Gallic acid-induced lung cancer cell death is related to glutathione depletion as well as reactive oxygen species increase. *Toxicol. in Vitro 24*, 1356−1362.
(38) Srour, Bilto YY, Juma, M., and Irhimeh, M. R. (2000) Exposure of human erythrocytes to oxygen radicals causes loss of deformability, increased osmotic fragility, lipid peroxidation and protein degradation. *Clin. Hemorheol. Microcirc. 23*, 13−21.